Published in final edited form as:
Magn Reson Med. 2014 October ; 72(4): 1176–1181. doi:10.1002/mrm.25027.

MRI under hyperbaric air and oxygen: effects on local magnetic field and relaxation times

Eric R. Muir[1,2], **Damon Cardenas**[2,5], **Shiliang Huang**[2], **John Roby**[2], **Guang Li**[2,4], and **Timothy Q. Duong**[1,2,3,4,6]

[1]Department of Ophthalmology, University of Texas Health Science Center, San Antonio, TX

[2]Research Imaging Institute, University of Texas Health Science Center, San Antonio, TX

[3]Department of Radiology, University of Texas Health Science Center, San Antonio, TX

[4]Department of Physiology, University of Texas Health Science Center, San Antonio, TX

[5]Department of Biomedical Engineering, University of Texas San Antonio, San Antonio, TX

[6]South Texas Veterans Health Care System, Department of Veterans Affairs.

Abstract

Purpose—Hyperbaric oxygen therapy has shown efficacies in the treatment of a number of diseases. The goal of this study was to develop a rodent hyperbaric chamber for MRI studies and to investigate the effects of hyperbaric air and hyperbaric oxygen on local magnetic field (B_0) and MRI relaxation parameters in the rat brain.

Methods—A hyperbaric chamber, constructed to fit inside a 7T animal MRI scanner, was pressurized with air to 4 atmospheres while oxygen was delivered locally via nose cone. B_0, T_2, T_2*, and T_1 maps in the rat brain were evaluated under normobaric air, hyperbaric air, and hyperbaric oxygen at 7T.

Results—Under hyperbaric oxygen, images exhibited artifacts and temporal instability, attributable to fluctuating oxygen concentration from air and oxygen mixing near the imaging region. Shielding the imaging region from fluctuating oxygen concentration resolved the problems. With increasing oxygen at hyperbaric pressure, B_0 was shifted downfield with increased inhomogeneity near the ear canals and nose. Brain T_2 and T_2* were lengthened, and T_1 was shortened.

Conclusion—This work establishes the means to perform MRI on rodents under hyperbaric conditions. Hyperbaric air and hyperbaric oxygen have significant effects on B_0 and tissue relaxation parameters compared to normobaric air.

Keywords

oxygen therapy; oxygen toxicity; BOLD; magnetic susceptibility; T1; T2; T2*; relaxation time constants

Correspondence: Timothy Duong, PhD, Research Imaging Institute, University of Texas Health Science Center, 8403 Floyd Curl Dr, San Antonio, TX 78229, duongt@uthscsa.edu, Tel 210 567 8100, Fax 210 567 8152.

INTRODUCTION

Hyperbaric oxygen (HBO) therapy has been used to treat decompression sickness, air embolism, chronic wounds, stroke, traumatic brain injury, and cerebral palsy, among others (1). While the direct effect of HBO exposure is increased tissue oxygenation, a number of therapeutic effects have been proposed, including stimulating release of factor promoting healing, decreased intracranial pressure and cerebral edema (1). Prolonged HBO exposure is however harmful. Non-invasive MRI could offer a means to study physiological effects, oxygen toxicity, and to monitor treatment efficacy during HBO. Moreover, functional imaging studies under HBO where both arterial and venous blood are saturated with oxygen could provide insight into the role of oxygen on the regulation of cerebral blood flow, oxygen metabolism, and neurovascular coupling.

Paramagnetic molecular oxygen has several effects on MRI parameters, including the static magnetic field (B_0), T_2, T_2*, and T_1 (2-9). Ambient oxygen gas alters B_0, which can lead to spatial shifts in MR images and fluctuations in signal intensity compared to air (2,3). Oxygen can also increase B_0 inhomogeneity near air-tissue interfaces such as near the ear canal and nasal cavity, which can lead to susceptibility artifacts, such as signal dropout and geometric distortion in echo-planar imaging (2). Moreover, [O_2] in the magnet bore could fluctuate when oxygen is delivered to the subjects, potentially affecting the temporal stability of MR signals.

Oxygen inhalation is known to increase blood T_2 and T_2* by increasing hemoglobin saturation, i.e., the blood-oxygen-level-dependent (BOLD) effect (5-7). Increased dissolved molecular oxygen in tissue and plasma water could also be expected to have a paramagnetic T_2 and T_2* shortening effect (2) but is normally masked by the BOLD effect. However, these paramagnetic effects of dissolved oxygen on T_2 and T_2* relaxation may not be negligible under HBO where even venous hemoglobin is saturated with oxygen (10). BOLD functional MRI, which detects functional activation via changes in deoxyhemoglobin content, could thus give weaker responses under HBO. Similarly, oxygen inhalation decreases brain parenchyma T_1 in the extravascular spaces as well as in blood plasma due to the paramagnetic dissolved oxygen (5,8,9,11). Such effects could complicate cerebral blood flow quantification using arterial spin labeling in which blood and tissue T_1 are important factors (9).

The goal of this study was to develop a rodent hyperbaric chamber for MRI studies and use it to investigate the effect of HBO on MRI relaxation properties and magnetic field. The challenges and solutions to designing the hyperbaric chamber are detailed. The hyperbaric chamber was used to investigate B_0, T_2, T_2*, and T_1 in the rat brain under normobaric air (NBAir), hyperbaric air (HBAir), and HBO conditions.

METHODS

Hyperbaric Chamber

A custom-made hyperbaric chamber for rodent MRI consisted of an animal cradle placed into a PVC pipe with O-rings on both ends of the cradle to provide a tight seal with the pipe

(**Figure 1a**). A threaded cap that screwed onto the pipe was used to hold the cradle in place in the pipe. The chamber was pressure tested with water up to 5 atm absolute (ATA). Coaxial radiofrequency cables were connected through the endplate via SMA adapters. Lines of physiological monitoring equipment (temperature probe and pulse oximeter) were passed through a large hole in a bundle and sealed with silicone sealant or glue. Animal temperature was maintained with circulating warm water through a winding of rigid plastic tubing with the inlet and outlet passed through tight-fitting holes in one of the endplates.

Four gas lines, made of rigid plastic tubing, were pushed through very tight-fitting holes at the endplates. The chamber was pressurized with air to 4 ATA through one line with the input near one end. A second line on the opposite end of the chamber was open to the atmosphere outside the chamber to vent gasses from the chamber and to allow continuous airflow. A valve was put in the vent line outside the chamber to adjust the flow rate of the vent and thus the chamber pressure. A third gas line was used to deliver oxygen (or air) to the animal via a tightly fit nose cone with excess gas directed to the outflowing vent away from the head. The fraction of oxygen in the vented gas was maintained at < 30% O_2 by adjusting flow rate of the pressurized air and the vent to avoid potential risk of explosion from concentrated pressurized oxygen in the chamber. Air was given through the nose cone when oxygen was not. The flow rate into the nose cone was set to 1.5 L/min. The fourth line was connected to a pressure meter to measure the chamber pressure.

In separate experiments outside the MRI, a small tube was inserted to sample the gas in the outlet of the nose cone. The gas was sampled at low flow rates to minimize perturbing the venting of the chamber. The gas was collected in a small plastic bag at atmospheric pressure. The percent oxygen in the sampled gas was measured (SurgiVet Capnograph, Smiths Medical PM Inc., Norwell, MA) after a steady reading was achieved over several minutes. We found that under our experimental HBO setup, the O_2 readings was >90-93%

Animal Preparation

The animal protocol was approved by the local Institutional Animal Care and Use Committee. Male Sprague-Dawley rats (n = 13, 254-600 g) were anesthetized with 1.5 g/kg urethane i.p. and imaged under spontaneous breathing conditions. Respiration rate, heart rate, and arterial oxygen saturation were monitored (MouseOx, STARR Life Science Corp., Oakmont, PA), and rectal temperature was maintained at 37±0.5 °C with a feedback-regulated circulating warm water pad. Inhaled anesthetics, blood pressure, and blood-gas measurement were not attempted due to hyperbaric conditions. Animals were placed into a head holder with ear and tooth bars, into the cradle, and then into the hyperbaric chamber. Animals were imaged under normobaric air (NBAir), hyperbaric air (HBAir), and hyperbaric oxygen (HBO) conditions. Each trial of HBO exposure was < 25 min to avoid possible oxygen toxicity effects (12) with similar periods of HBAir in between.

Magnetic Resonance Imaging

MRI was performed on a 7T magnet with 400 mT/m gradients (Bruker, Billerica, Massachusetts) and with a 2 cm transmit/receive surface coil. Global shimming was only performed once at the beginning of a session and was not repeated under different

conditions. Non-localized spectroscopy was used to measure frequency shifts of the water peak with TR = 300 ms, spectral width = 25 kHz, 6250 points zero-filled to 8192, and 160 repetitions. B_0 maps were acquired with a 3D multi-echo gradient-echo sequence with a field of view (FOV) = 25.6×25.6×30 mm^3, matrix = 64×64×75, TR = 20 ms, TE = 2.3 and 8.1 ms, and 3 averages. B_0 was acquired once and spectroscopy was repeated 1-3 times for each of the NBAir, HBAir, and HBO condition.

For T_2, multi-echo fast spin echo was used with FOV = 25.6×25.6 mm^2 and matrix = 96×96, seven 1.5 mm thick slices, TR = 3 s, effective TEs = 25, 40, 75, and 120 ms, echo train length = 8, and 4 averages. For T_2*, multi-echo gradient-echo was used with FOV = 25.6×25.6 mm^2 and matrix = 96×96, TR = 1.5 s, ten TEs from 3.1 to 22.9 ms equally spaced by 2.2 ms, and 2 averages. Fourteen 0.75 mm thick slices were acquired and consecutive pairs averaged to give seven 1.5 mm thick slices to minimize effects of through-plane dephasing. For T_1, inversion-recovery gradient-echo echo planar imaging was used with FOV = 25.6×25.6 mm^2 and matrix = 96×96, seven 1.5 mm thick slices, TR = 12 s, TE = 9.9 ms, ten inversion times from 23 to 3623 ms equally spaced by 400 ms, 2/3 partial Fourier acquisition, and 3 averages.

MRI Analysis

Image analysis was done using Matlab (MathWorks, Natick, MA) and Statistical Parametric Mapping 5 (SPM5) software. B_0 maps in Hz were calculated with SPM5 from the image phase data. The realignment tool of SPM5 was used to measure the spatial shift in images due to hyperbaric conditions. T_2 maps were calculated using a linear fit of the logarithm of the data at different echo times, TE, to $\ln(M) = \ln(M_0) - (TE/T_2)$. T_2* maps were calculated similarly after averaging pairs of 0.75 mm slices to give 1.5 mm thick slices. T_1 maps were calculated using a three-parameter non-linear fit of the data at different inversion times, TI, to $M = M_0 - B \cdot M_0 \cdot \exp(-TI/T_1)$, where M is the signal intensity at a given TI, M_0 is the equilibrium signal, and B is the efficiency of the inversion pulse.

Statistical Analysis

Group-average data are expressed as mean ± standard error of the mean (SEM) unless indicated otherwise. Relaxation time and frequency of the water peak were analyzed under NBAir, HBAir, and HBO conditions using analysis of variance followed by paired t-tests with Bonferroni-Holm correction for multiple comparisons. Corrected $P < 0.05$ was taken as statistically significant.

RESULTS

Artifacts from HBO and solutions

In our initial experience with MRI under HBO, most images exhibited artifacts. Moreover, the time-series images and the spectroscopic water frequencies and amplitudes were temporally unstable. Such instability was verified not to be physiological by repeating studies in phantoms and dead animals, which showed similar instability (**Figure 2**, dotted red lines). Fluctuating $[O_2]$ around the imaging region (i.e., the head) under HBO was suspected to be the cause of such instability. A solution was implemented by i) covering the

space around the head with a head cover made from hot melt adhesive to act as a barrier to the mixing of oxygen (from the nose cone) and air (from the end of the chamber) around the head, and ii) by tightly fitting the cone on the nose with excess gas diverted away from the animal toward the vent outlet (**Figure 1b,c**). The MRI results of such solution are also shown in **Figure 2** (solid black lines). The instability was predominantly resolved. With the solution implemented, minor image artifacts and minor temporal instability under HBO, although tolerable, were observed occasionally in live animals but never in dead animals. This effect was attributed to enhanced physiological (respiratory) noise.

Effects of hyperbaric conditions on B_0

At steady state, the water spectroscopic frequencies under NBAir, HBAir, and HBO were all significantly different from each other (corrected $P < 0.05$). The frequency differences between HBAir-NBAir and HBO-NBAir were −6.8 ± 1.0 and −28.5 ± 6.3 Hz, respectively (live animal, n = 4). B_0 maps in Hz showed spatially heterogeneous frequency differences between conditions (**Figure 3**). Between NBAir and HBAir, the largest differences were around the ear canals. Between HBAir and HBO, the largest difference occurred around the olfactory bulb and anterior brain structures due to the delivery of oxygen through the nose cone. The B_0 changes due to oxygen resulted in spatial shifts in the images. The brain was shifted in the phase encode (dorsal-ventral) direction by ~0.9-1.8 pixels going from NBAir to HBAir and by <0.1 up to 0.3 pixels from HBAir to HBO. Spatial shifts in the frequency encode (left-right) direction was negligible, <0.1 pixels. There were also subtle changes in shape and the extent of signal dropout of the brain going from normobaric air to hyperbaric conditions (data not shown).

Effects of hyperbaric conditions on animal physiology, T_2, T_2*, and T_1

Table 1 shows animal physiological parameters under NBAir, HBAir and HBO. Respiration and heart rates were reduced during HBAir and HBO compared to NBAir, but similar between HBAir and HBO. Whole-brain T_2, T_2*, and T_1 values during NBAir, HBAir, and HBO are shown in **Figure 4**. T_2 and T_2* were lengthened by HBAir and HBO compared to NBAir, while T_1 was shortened. In contrast to T_1 and T_2*, T_2 maps were not susceptible to fluctuating oxygen under HBO even without shielding. T_2 values were not significantly different between with and without shielding ($P = 0.31$, t-test).

DISCUSSION

This study describes the construction of a hyperbaric chamber for rodent MRI under hyperbaric air and oxygen. HBO was achieved using air to pressurize the chamber with a separate line to deliver oxygen locally to the animal's nose to prevent risks of explosion associated with highly concentrated oxygen. This implementation however leads to fluctuating oxygen levels around the imaged object, causing frequency and amplitude fluctuations, which results in image degradation and temporal instability. The solution was to shield the space around the imaged region and divert excess oxygen away from it. Such temporal instability was negligible under HBAir.

With the solution as described, some minor artifacts during HBO exposure were still observed infrequently in T_1, T_2*, and B_0 images in live animals but never in dead animals (n = 6 for T_2* and n = 2 for T_1). This observation suggests another source of artifacts in live animals, such as enhanced physiological noise. For example, respiratory noise from variation in magnetic susceptibility in the chest during the respiration (13) could be exacerbated by the high paramagnetic oxygen concentration in the lung under HBO given that HBAir data were free of artifacts. Physiological noise could be minimized by using gating, retrospective correction, or navigator echoes in future studies (14,15). Additionally, fast spin-echo acquisition can be used as it was less susceptible to the oxygen fluctuations even without shielding.

Effects on B_0

Under steady-state hyperbaric conditions, the increased ambient oxygen shifted the water frequency, resulting in a position shift relative to NBAir, which can be readily corrected by image co-registration. Hyperbaric conditions also created magnetic field inhomogeneity in the nose region and ear canal because of the ambient oxygen around these air-tissue interfaces. From NBAir to HBAir, magnetic field inhomogeneity increased in the ear canal as expected. Similar shielding around the ear or using filler (such as toothpaste) in the ear canal can also be applied to the ear regions to avoid field inhomogeneity. From HBAir to HBO, magnetic field inhomogeneity increased in the nose regions, affecting the olfactory bulb and anterior brain. B_0 field maps could be used to correct the field inhomogeneity. The effect of ambient oxygen on B_0 has been shown to have undesirable consequences in various MR applications, such as altering image intensity in BOLD fMRI of hyperoxic inhalation (2,3) or altering phase in MR thermometry and phase-contrast MR angiography (4).

Effects on T_2, T_2*, and T_1

Compared to normobaric air, air at 4 ATA would have 4 times the oxygen, NBO would have 4.76 times the oxygen, and pure oxygen at 4 ATA would be expected to have 19 times the oxygen content. We measured the percent O_2 in the outlet of the nose cone to be around 90%, suggesting our experimental conditions were close to achieving the ideal of 100% oxygen at hyperbaric pressure. Since HBAir at 4 ATA has similar [O_2] as NBO, we expect these conditions would have similar effects on relaxation parameters. However, whole-brain T_2 increased by 1% during HBAir compared to NBAir, which was smaller than previous reported T_2 increases of 4-16% in mice at 9.4T (5) and 3-12% in rats at 7T (6) during NBO compared to NBAir. Whole-brain T_2 increased by only 2% during HBO compared to NBAir. Similarly, whole-brain T_2* increased during HBAir by 7% and during HBO by 8%, which are also smaller than a previous study reporting brain T_2* increased by 13-23% in rats at 7T during NBO compared to NBAir (6). Experimental conditions such as field strength, species, anesthesia (pentobarbital/urethane (5) or chloral hydrate (6)), and whether animals were mechanically ventilated (6) or not (5) do not appear to have noticeable effects on the T_2 changes. Additionally, the regions of interest analyzed may affect the results, with large differences between ROIs within the same studies (5,6).

In addition to affecting T_2 and T_2* through hemoglobin, dissolved paramagnetic oxygen in the blood and tissue should also have a direct T_2 and T_2* shortening effect (2). Under

normobaric air conditions, the BOLD effect from deoxyhemoglobin is dominant (5,6). With sufficiently high dissolved blood oxygen when hemoglobin is saturated, the BOLD effect may also become saturated and the relaxation enhancement effect could begin to counteract it. Venous hemoglobin saturation is only 87% (pO_2 = 57 mmHg) under NBO but is essentially 100% (pO_2 = 424 mmHg) under HBO at 3 ATA (10). The changes in T_2 and T_2* herein tended to be smaller going from HBAir to HBO than from NBAir to HBAir, suggesting the BOLD effect was possibly saturated. Functional MRI BOLD contrast could thus be reduced at HBO.

Whole-brain T_1 was shortened during HBAir by 2% compared to NBAir, which is similar to or smaller than some previously reported T_1 decreases of 4-11% in mice at 9.4T (5), 3-7% in rats at 7T (6), and 2% in rats at 7T (8) during NBO compared to NBAir. Whole-brain T_1 was shortened during HBO by 7% compared to NBAir, substantially smaller than expected based on the assumed [O_2] differences between NBAir and HBO. HBO-induced T_1 shortening could have implications in blood flow quantification using arterial spin labeling MRI (9). Arterial pO_2 under HBO is >2000 mmHg (10,16,17) which would significantly alter arterial T_1, substantially increasing the rate at which the label signal decays in blood and increasing the difference between arterial T_1 and tissue T_1, confounding blood flow quantification by arterial spin labeling. Blood T_1 and cerebral blood flow measurements under HBO are currently under investigation. T_1 measurement has been used to evaluate oxygen tension in body fluids such as cerebrospinal fluid and vitreous under normobaric conditions (11,18) and it could also be applied to hyperbaric conditions.

Conclusions

This study described the design of a rodent hyperbaric chamber for MRI studies and demonstrates the feasibility of performing MRI during hyperbaric air and oxygen. Under hyperbaric oxygen conditions, there were image artifacts from the rapid fluctuations in oxygen levels due to mixing of air and oxygen at hyperbaric pressures. Solutions were implemented to minimize image artifacts. Hyperbaric air and hyperbaric oxygen showed significant effects on B_0 and tissue relaxation parameters compared to normobaric air.

Acknowledgments

Grant support: This work was supported in part by the NIH/NINDS (R01 NS45879) and by NIH T32HL007446.

Abbreviations

HBO	hyperbaric oxygen
NBO	normobaric oxygen
HBAir	hyperbaric air
NBAir	normobaric air
ATA	atmospheres absolute
BOLD	blood oxygen level dependent

SEM	standard error of the mean
SD	standard deviation

References

1. Al-Waili NS, Butler GJ, Beale J, Abdullah MS, Hamilton RW, Lee BY, Lucus P, Allen MW, Petrillo RL, Carrey Z, Finkelstein M. Hyperbaric oxygen in the treatment of patients with cerebral stroke, brain trauma, and neurologic disease. Adv Ther. 2005; 22:659–678. [PubMed: 16510383]
2. Pilkinton DT, Gaddam SR, Reddy R. Characterization of paramagnetic effects of molecular oxygen on blood oxygenation level-dependent-modulated hyperoxic contrast studies of the human brain. Magn Reson Med. 2011; 66:794–801. [PubMed: 21608026]
3. Bates S, Yetkin Z, Jesmanowicz A, Hyde JS, Bandettini PA, Estkowski L, Haughton VM. Artifacts in functional magnetic resonance imaging from gaseous oxygen. J Magn Reson Imaging. 1995; 5:443–445. [PubMed: 7549208]
4. Streicher MN, Schafer A, Reimer E, Dhital B, Trampel R, Ivanov D, Turner R. Effects of air susceptibility on proton resonance frequency MR thermometry. MAGMA. 2012; 25:41–47. [PubMed: 21479876]
5. Uematsu H, Takahashi M, Hatabu H, Chin CL, Wehrli SL, Wehrli FW, Asakura T. Changes in T1 and T2 observed in brain magnetic resonance imaging with delivery of high concentrations of oxygen. J Comput Assist Tomogr. 2007; 31:662–665. [PubMed: 17895773]
6. Wu Y, Gao X, Feng X, Tao X, Tang CY. Oxygen-enhanced magnetic resonance imaging of the brain: a rodent model. Neuroreport. 2012; 23:581–584. [PubMed: 22648394]
7. Remmele S, Sprinkart AM, Muller A, Traber F, von Lehe M, Gieseke J, Flacke S, Willinek WA, Schild HH, Senegas J, Keupp J, Murtz P. Dynamic and simultaneous MR measurement of R1 and R2* changes during respiratory challenges for the assessment of blood and tissue oxygenation. Magn Reson Med. 2013; 70:136–146. [PubMed: 22926895]
8. Shen Q, Huang S, Du F, Duong TQ. Probing ischemic tissue fate with BOLD fMRI of brief oxygen challenge. Brain Res. 2011; 1425:132–141. [PubMed: 22032876]
9. Pilkinton DT, Hiraki T, Detre JA, Greenberg JH, Reddy R. Absolute cerebral blood flow quantification with pulsed arterial spin labeling during hyperoxia corrected with the simultaneous measurement of the longitudinal relaxation time of arterial blood. Magn Reson Med. 2012; 67:1556–1565. [PubMed: 22135087]
10. Whalen RE, Saltzman HA, Holloway DH Jr. McIntosh HD, Sieker HO, Brown IW Jr. Cardiovascular and Blood Gas Responses to Hyperbaric Oxygenation. Am J Cardiol. 1965; 15:638–646. [PubMed: 14285147]
11. Zaharchuk G, Busse RF, Rosenthal G, Manley GT, Glenn OA, Dillon WP. Noninvasive oxygen partial pressure measurement of human body fluids in vivo using magnetic resonance imaging. Acad Radiol. 2006; 13:1016–1024. [PubMed: 16843855]
12. Bitterman N, Melamed Y, Perlman I. CNS oxygen toxicity in the rat: role of ambient illumination. Undersea Biomed Res. 1986; 13:19–25. [PubMed: 3705247]
13. Raj D, Paley DP, Anderson AW, Kennan RP, Gore JC. A model for susceptibility artefacts from respiration in functional echo-planar magnetic resonance imaging. Phys Med Biol. 2000; 45:3809–3820. [PubMed: 11131201]
14. Glover GH, Li TQ, Ress D. Image-based method for retrospective correction of physiological motion effects in fMRI: RETROICOR. Magn Reson Med. 2000; 44:162–167. [PubMed: 10893535]
15. Le TH, Hu X. Retrospective estimation and correction of physiological artifacts in fMRI by direct extraction of physiological activity from MR data. Magn Reson Med. 1996; 35:290–298. [PubMed: 8699939]
16. Clark JM, Lambertsen CJ. Alveolar-arterial O2 differences in man at 0.2, 1.0, 2.0, and 3.5 Ata inspired PO2. J Appl Physiol. 1971; 30:753–763. [PubMed: 5572798]

17. Weaver LK, Howe S. Normobaric measurement of arterial oxygen tension in subjects exposed to hyperbaric oxygen. Chest. 1992; 102:1175–1181. [PubMed: 1395764]

18. Muir ER, Zhang Y, San Emeterio Nateras O, Peng Q, Duong TQ. Human Vitreous: MR Imaging of Oxygen Partial Pressure. Radiology. 2013; 266:905–911. [PubMed: 23220896]

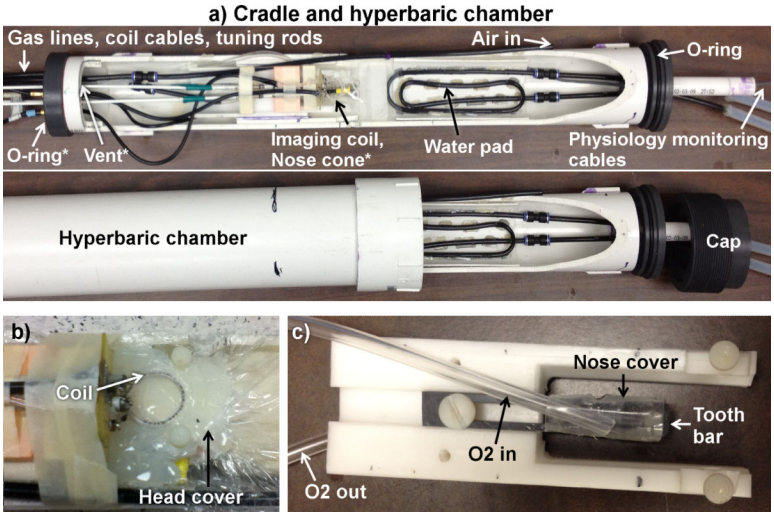

Figure 1.

(a) MRI compatible hyperbaric chamber for rodents that is made of PVC. The animal holder with a head holder is placed into the chamber. Cables of the coils, gas lines, and lines of physiological monitoring equipment are passed through tight fitting holes on the two ends of the cradle. Air to pressurize the chamber is delivered through the line labeled “Air in.” A separate gas line directly delivers oxygen via the nose cone to the animal (underneath the imaging coil). The “vent’ is open to the atmosphere outside the chamber, allowing continuous air flow through the chamber. A seal between the cradle and chamber was made with o-rings on both ends of the cradle. When the cradle was pushed all the way into the chamber, the cap screwed into the end of the hyperbaric chamber to hold the cradle tightly in place. (b) The head cover to block the mixing of oxygen and air around the head to minimize oxygen fluctuation. (c) The headset and the tight fitting nose cone with excess gas diverted away from the animal toward the vent outlet. The “O2 out” line is connected to the hole in the tooth bar for the animal's teeth and to the vent. *Indicates the location of objects that are not visible in the image.

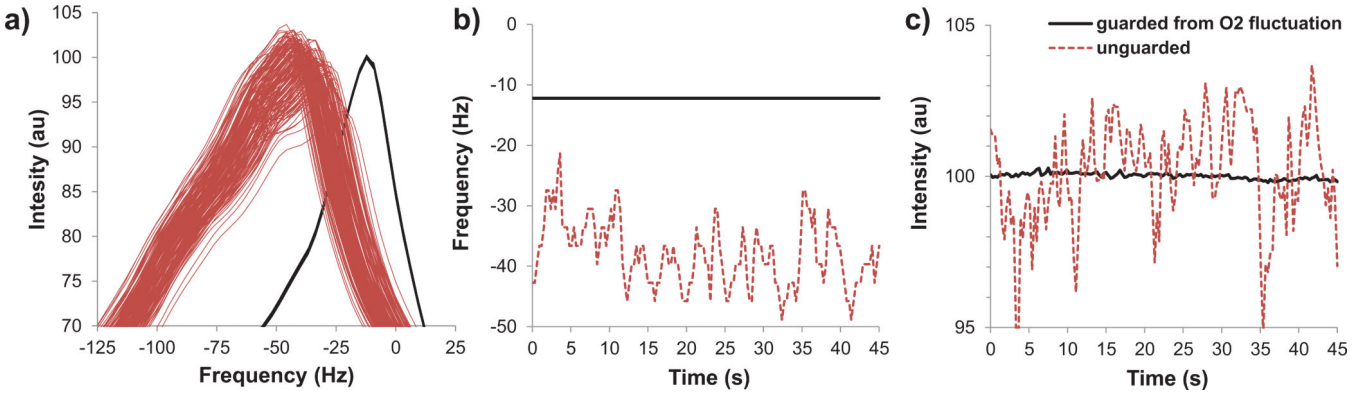

Figure 2.

Temporal fluctuations of $^{1}H_2O$ spectra during HBO in dead animals without (red dashed lines) and with the head cover and nose cone (solid black lines) to guard from oxygen fluctuations. (a) Frequency resonance, (b) peak frequency, and (c) peak intensity across time. The temporal fluctuations were eliminated with the head cover and nose cone. Under NBAir and HBAir spectra are similar to the "guarded from O_2 fluctuation" data.

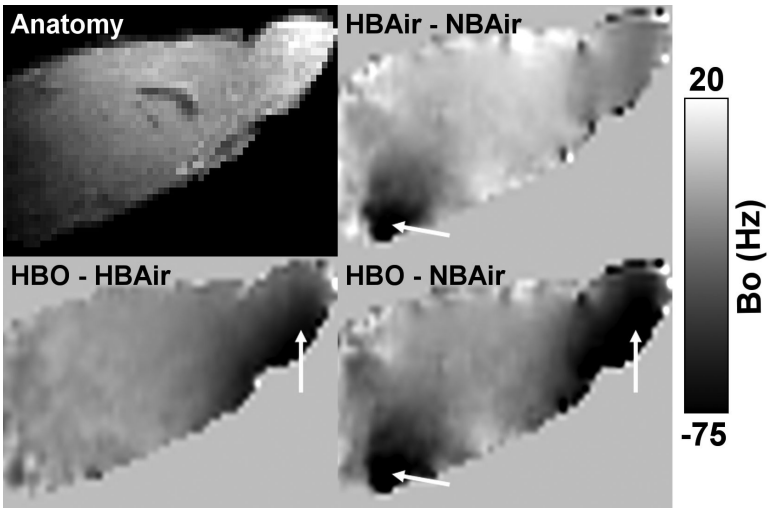

Figure 3.

B_0 difference maps in Hz between NBAir, HBAir, and HBO from a mid-sagittal slice with an anatomical image for reference. Frequency overall is negative with increasing oxygen with the largest changes near the ear canals and olfactory bulb (arrows).

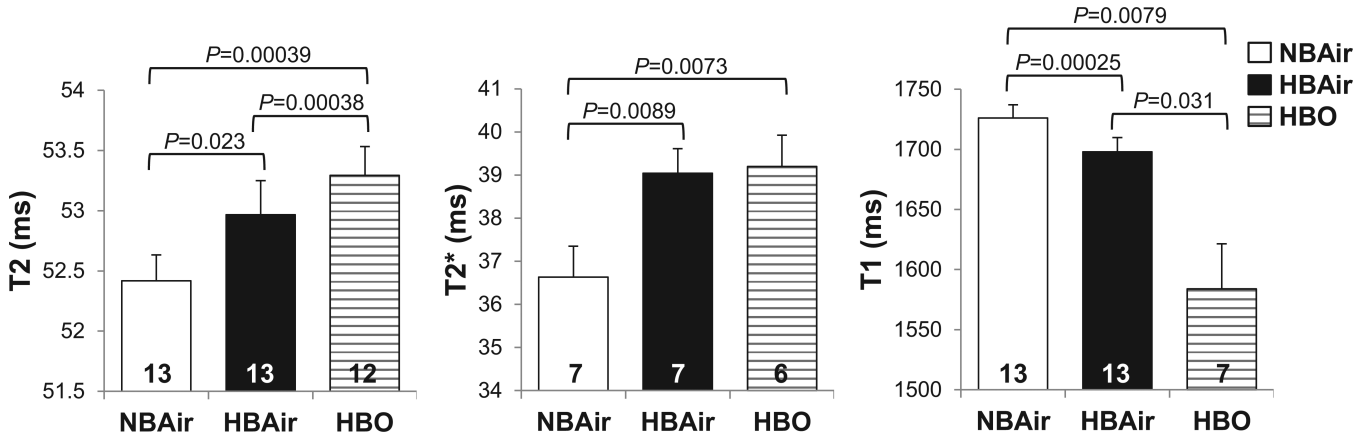

Figure 4.

Whole-brain T_2, T_2*, and T_1 during NBAir, HBAir, and HBO (mean ± SEM, n shown at the bottom of each bar). Significant differences are indicated by the brackets with given uncorrected *P*-values. T_1 and T_2* data acquired during HBO without shielding were excluded from analysis due to artifacts. Furthermore, T_2* HBO data were discarded in one animal with shielding in which the T_2*-weighted images still had significant artifacts.

Table 1

Physiological parameters in animals, mean ± SD (n). The smaller sample sizes for HBAir and HBO is due to loss of the respiration signal from the oximeter.

	NBAir	HBAir	HBO
Respiration Rate in breaths/min	121 ± 14 (6)	101 ± 19* (4)	115 ± 4 (3)
Heart Rate in beats/min	387 ± 37 (10)	360 ± 28* (10)	350 ± 22* (9)
SpO_2 in %	95.0 ± 1.9 (10)	98.4 ± 0.5* (10)	98.4 ± 0.5* (9)

* $P < 0.05$ compared to NBAir from paired t-test